Hindawi
Advances in Materials Science and Engineering
Volume 2024, Article ID 6681559, 15 pages
https://doi.org/10.1155/2024/6681559

Research Article

Efficient Bioelectrochemical Cell Generation and Green Synthesis of Silver Nanoparticles Using Pomegranate and Pineapple Peel Extracts: A Comprehensive Characterization Study

Shamima Mehrin,[1] **Nilufer Yesmin Tanisa**,[1] **Rabiul Awal**,[1] **Md. Kamrul Alam Khan**,[2] **Abdus Shaqur**,[1] **Shamim Ahmed**,[1] **Shahidul Islam**,[3] **and Asad Mia**[1]

[1]*Department of Physics, Uttara University, Uttara, Dhaka 1230, Bangladesh*
[2]*Department of Physics, Jagannath University, Dhaka 1100, Bangladesh*
[3]*Bangladesh Atomic Energy Regulatory Authority, Dhaka 1207, Bangladesh*

Correspondence should be addressed to Shamima Mehrin; 2231121007@uttarauniversity.edu.bd

Received 14 December 2023; Revised 17 January 2024; Accepted 18 March 2024; Published 28 March 2024

Academic Editor: Gianfranco Carotenuto

The present study investigates an environmentally conscious method for synthesizing silver nanoparticles (AgNPs) by employing extracts from pomegranate peel (PgP) and pineapple peel (PnP). This green synthesis approach offers a sustainable alternative to traditional chemical methods, thereby reducing the ecological footprint associated with nanoparticle production. The PgP and PnP extracts serve as both reducing and capping agents during the synthesis process, enhancing the biocompatibility of the resultant AgNPs. Various characterization techniques, including UV-Vis spectroscopy, Raman analysis, X-ray diffraction (XRD), dynamic light scattering (DLS), Fourier transform infrared (FTIR), and transmission electron microscopy (TEM), were utilized to analyze the synthesized AgNPs. UV-Vis spectroscopy confirmed the formation of AgNPs through characteristic surface plasmon resonance peaks, while FTIR examined the interaction between biomaterial components and the oxidation and coating of silver nanoparticles. Raman analysis elucidated the functional groups responsible for reducing and stabilizing AgNPs, while XRD provided insights into their crystalline structure. TEM images revealed the size and morphology of the nanoparticles, while DLS characterized their average size and morphology. In addition, the synthesized AgNPs were utilized in a bioelectrochemical cell to leverage their unique properties for enhanced electrochemical performance, showcasing their potential application in energy storage and conversion systems. Overall, this study demonstrates the feasibility of utilizing agricultural waste products such as PgP and PnP for sustainable AgNP synthesis, offering promising prospects for environmentally friendly nanotechnology advancement.

1. Introduction

Metal nanoparticles display distinctive optical and optoelectronic characteristics within the size range of 1–100 nm. As a result, they have been extensively utilized across diverse domains, including catalysis, electronics, optics, environmental science, and biotechnology. This has led to a sustained and ongoing interest in their applications [1–4]. In recent years, the field of nanotechnology has witnessed a paradigm shift towards sustainable and eco-friendly approaches for the synthesis of nanoparticles [5].

The exploration of green synthesis methods has gained significant attention due to their inherent advantages over conventional chemical methods, such as reduced environmental impact, cost-effectiveness, and the use of renewable resources. One promising avenue in this context involves the utilization of plant extracts as reducing and stabilizing agents for the fabrication of nanoparticles. Among the various botanical sources, pineapple (*Ananas comosus*) and pomegranate (*Punica granatum*) peel extracts have emerged as compelling candidates for the green synthesis of silver nanoparticles (AgNPs).

One notable avenue in the realm of green synthesis involves the utilization of PgP and PnP as potent bioreducing and capping agents for the synthesis of AgNPs. PgP and PnP, often regarded as agricultural waste, have been recognized for their rich content of bioactive compounds, including polyphenols, flavonoids, and enzymes [6]. These bioactive constituents play a pivotal role in the reduction of silver ions and stabilization of the resulting nanoparticles, rendering the synthesis process not only environmentally benign but also cost-effective.

Silver nanoparticles (AgNPs) have been produced from diverse plant parts such as roots, seeds, leaves, stems, and flowers, serving various purposes, particularly in biomedical applications [7]. For example, AgNPs were synthesized using aqueous extracts from plants such as *Cleome viscosa, Origanum vulgare, Ocimum tenuiflorum, Solanum trilobatum, Syzygium cumini, Impatiens balsamina, Lantana camara*, and *Centella asiatica*, demonstrating antibacterial properties [7–10]. The authors in [11] utilized the root extract of Cyperus scariosus to synthesize gold nanoparticles (AuNPs) and investigated their potential applications in degrading methylene blue (MB) dye and sensing Ni^{2+} in water. In previous studies, *Gelidium amansii, Enteromorpha compressa, Phanerochaete chrysosporium, Bacillus brevis*, and *Daucus carota* have also been utilized for AgNP biosynthesis, with researchers investigating their antimicrobial properties [12]. The authors in [13] researched synthesized ED-AgNPs, revealing heightened antimicrobial efficacy. The study demonstrated greater effectiveness against Gram-positive bacteria (e.g., *L. monocytogenes* with an inhibition zone of 18 mm) compared to Gram-negative bacteria (e.g., *E. coli* with an inhibition zone of 10 mm). In another investigation, the authors in [14] explored the synthesis of hydroxyethylcellulose phthalate-functionalized silver nanoparticles (HEC-PA@AgNPs) through an environmentally friendly approach, employing sunlight exposure for just a few seconds. Furthermore, the authors in [15] delved into the synthesis and characterization of adipic acid-capped silver nanoparticles (AgNPs@AA), highlighting their antimicrobial activities. The study also investigated their application in selectively detecting Hg^{2+} ions in aqueous solutions. The green synthesis of AgNPs using PnP [16] and PgP [17] offers several advantages, including scalability, biocompatibility, and the absence of hazardous chemicals. The choice of these fruit peels as reducing agents is rooted in their inherent ability to facilitate the reduction of silver ions, leading to the formation of well-defined nanoparticles with controlled size and morphology. The bioreduction process is often accompanied by additional biofunctionalization, imparting unique properties to the AgNPs that can be tailored for specific applications [18]. The authors in [19] researched synthesizing silver nanoparticles (AgNPs) by utilizing a polar extract obtained from Cotoneaster nummularius leaves. Furthermore, the authors in [20] presented a groundbreaking method involving the application of olive fruit extract for the green synthesis of AgNPs, achieved through sunlight irradiation lasting only tens of seconds. Numerous *in vitro* experiments have illustrated the substantial antimicrobial capabilities of silver nanoparticles (AgNPs). Some of these investigations have underscored their potential to overcome resistance exhibited by certain bacterial strains [21, 22]. In addition, AgNPs have been found to play a role in anticancer therapy by inducing apoptosis and facilitating the targeted delivery of antineoplastic agents to cancer cell sites [23]. Although the precise mechanisms behind the bactericidal and cytotoxic effects remain unclear, there is sufficient compelling evidence in the literature to indicate that the method of synthesis and the reducing agents employed in their synthesis significantly contribute to determining the level of toxicity and antimicrobial effectiveness of AgNPs [24]. The authors in [25] reported the facile synthesis of silver nanoparticles via sunlight irradiation of an AgNO3 solution and 4-(phenylsulphonamido)benzoic acid (PSBA). This research aims to generate and characterize silver nanoparticles (AgNPs) by utilizing PgP and PnP extracts. The production process involves controlled reduction of the initial AgNP substance, where the PgP and PnP extract serve the dual purpose of reducing and covering. Various analytical techniques, such as X-ray diffraction (XRD), UV-Vis spectroscopy analysis, Raman analysis, transmission electron microscope (TEM), DLS analysis, and Raman analysis, are employed to comprehensively examine the resulting nanoparticles, assessing their size, arrangement, composition, and durability.

In summary, this study highlights the impressive efficacy of Ag nanoparticles utilizing PgP and PnP extracts in bioelectrolyte power generation systems, presenting a straightforward, cost-effective, and environmentally friendly approach for AgNPs synthesis. Thus, the potential of AgNPs for PgP and PnP to provide a novel foundation for the development of bioelectrochemical cells is underscored, emphasizing the need to explore their impact on these cells.

2. Techniques and the Systematic Approach

2.1. Substances and Components. Silver nitrate was acquired from Confidence Scientific CO. Ltd, Hatkhola road, Bangladesh. Pomegranate (*Punica granatum*) fruits and pineapple (*Ananas comosus*) fruits were sourced from a local supermarket in Uttara, Dhaka, Bangladesh. All solutions were prepared using distilled water, and glassware was meticulously cleaned with distilled water and oven-dried before usage.

2.2. The Generation of Extracts. To minimize dust contamination, the PgP underwent a thorough cleaning process. This involved reducing dust particles through separate washings of the PgP and PnP with deionized (DI) water, followed by air drying at room temperature. Subsequently, the dried PgP and PnP were individually ground into extracts using grindstones. Each extract, consisting of 50 grams of PgP and PnP, was combined with 200 milliliters of deionized water. The mixture was then agitated on a hot plate set at 64°C for 30 minutes using a magnetic stirrer. After cooling to room temperature, the PgP and PnP extracts were obtained by filtering the mixtures through Whatman 41 paper to remove any remaining solids. Finally, the extracts

were stored separately at 3°C for 50 minutes. The PgP and PnP were stored at 4°C in the refrigerator until further use in the experiment.

2.3. Environmentally Friendly Production of Silver Nanoparticles. To commence the trial, a 30 mL solution of $AgNO_3$, having a concentration of 1.0 mM, was prepared in a 100 mL conical flask. Following this, 9 mL of extracts from PgP and PnP were delicately introduced into the solution separately. After gently agitating the mixtures, they were left to incubate in darkness for a duration of 70 minutes. Within this timeframe, a noticeable color change occurred, with the PgP transforming from orange to deep maroon and the PnP changing from light pink to red. After several days, the PgP extract solution darkened, and black sediment accumulated at the volumetric flask's bottom whereas the PnP extract solution water colored, and black sediment accumulated at the volumetric flask's bottom, confirming the successful synthesis of Ag nanoparticles. Figure 1 depicts the procedural steps for producing Ag nanoparticles from (a) PgP extract and (b) PnP extract. Figure 2 shows the color change in the solution after the addition of (a) PgP extract and (b) PnP due to the reduction of silver ions.

2.4. The Core Concept behind a Synopsis Cell. Cell structures were constructed by utilizing zinc and copper electrodes, and the electrolyte consisted of a solution containing fluids extracted from PgP and PnP separately. The reaction was aided by naturally occurring silver nanoparticles, serving as catalysts with environmental origins. The role of the copper electrode was to act as an electron collector, transferring electrons to the zinc sheet, and thereby initiating interactions with hydrogen ions and Cu^{2+} ions within the system. As a result, these ions underwent a gradual transformation, leading to the production of H_2 gas and the deposition of copper atoms onto the copper electrode. Over time, the cells consistently released H_2 gas, and copper atoms progressively accumulated on the copper electrode.

2.5. Designing Nanoparticle Cell Structures. Three distinct organic cells were established to investigate the impact of silver nanoparticles on energy generation processes. In the initial configuration depicted in Figure 3(a), zinc and copper sheets served as conductors, with identical lower sections. The cell's electrolyte consisted of a blend of 100 ml each of PgP extract. Progressing to Figure 3(b), zinc and copper plates were employed as conductors, incorporating 100 ml of PgP extract, along with 9 ml of $CuSO_4.5H_2O$ individually. Moving forward to Figure 3(c), the electrolyte comprised a 100 mL solution of PgP extract, exposed to 9 ml of $CuSO_4.5H_2O$, and a separate 50 ml dose of a silver nanoparticles blend. In Figure 3(d), zinc and copper sheets served as conductors, with identical lower sections. The cell's electrolyte consisted of a blend of 100 ml each of PnP extract. Progressing to Figure 3(e), zinc and copper plates were employed as conductors, incorporating 100 ml of PnP extract, along with 9 ml of $CuSO_4.5H_2O$ individually. Moving forward to Figure 3(f), the electrolyte comprised a 100 mL solution of PnP extract, exposed to 9 ml of $CuSO_4.5H_2O$, and a separate 50 ml dose of a silver nanoparticles blend. Figure 3 illustrates an experimental setup designed to evaluate the fundamental concept of cells utilizing zinc or copper components, incorporating PgP and PnP extracts, and varying concentrations of silver nanoparticles.

2.6. Functional Roles of Silver Nanoparticles in Energizing Processes. The active roles of Ag nanoparticle energy functions were examined in cases 1, 2, and 3, focusing on open circuit voltage and short-circuit current. The approach adopted included assessing the energy levels of different cells through the formula: $P = V_{oc} \times I_{sc}$. This same formula was applied for gauging the cells' resistance, denoted as $R_{in} = V_{oc}/I_{sc}$. To elaborate, in this context,

P signifies the cell's power.

R_{in} denotes the internal resistance of the cell.

2.7. Bioelectrochemical Cell Chemical Reaction. Figure 4 depicts a bioelectrochemical cell. In this case, Zn serves as a sacrificial element, acting as a cathode, while Cu serves as an anode.

2.7.1. Chemical Reactions

(1) Zn reaction:

$Zn = Zn^{2+} + 2e^-$; here, zinc (Zn) undergoes oxidation to form zinc ions (Zn^{2+}) and release electrons. This reaction is typical of sacrificial anodes, where zinc acts as the sacrificial element, corroding instead of other metals.

Cu reaction:

$Cu^{++} + 2e^- = Cu$; in this reaction, copper ions (Cu^{2+}) gain electrons to form solid copper. Copper serves as the cathode in this electrochemical system.

Now, the addition of these two reactions is described as follows:

$$Zn + Cu^{2+} = Zn^{2+}. \quad (1)$$

Where Cu^{2+} = ion that reacts and Zn^{2+} = ionization of the product.

(2) Zinc with hydrogen ions:

$Zn = Zn^{2+} + 2e^-$, where, Zn^{2+} = ionization of the product

At extract: $2H^+ + 2e^- = H_2$

Where, H^+ = ion that reacts

Adding,

$$Zn + 2H^+ = Zn^{2+} + H_2, \quad (2)$$

Where H^+ = ion that reacts and Zn^{2+} = ion that reacts.

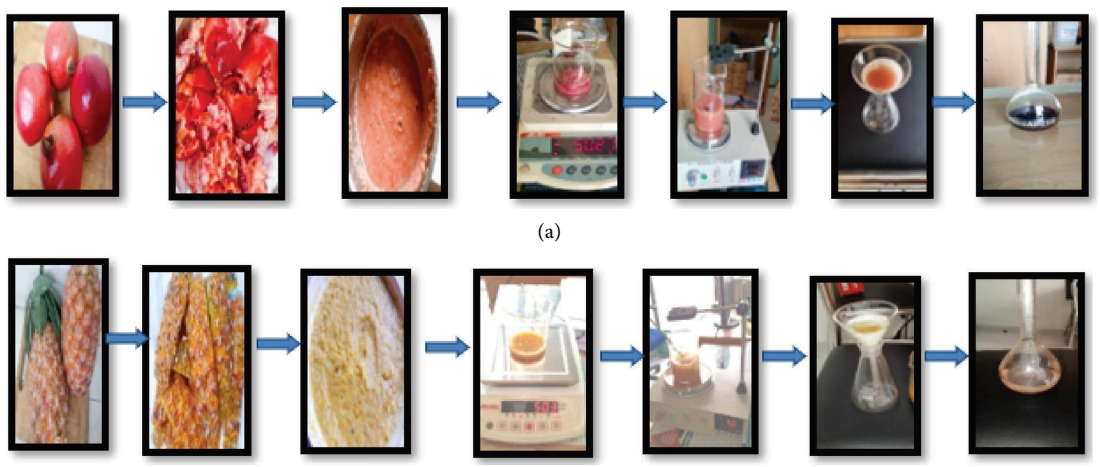

(a)

(b)

Figure 1: The procedural steps for producing Ag nanoparticles from (a) PgP extract and (b) PnP extract.

(a) (b)

Figure 2: Color change in the solution after the addition of (a) PgP extract and (b) PnP due to the reduction of silver ions.

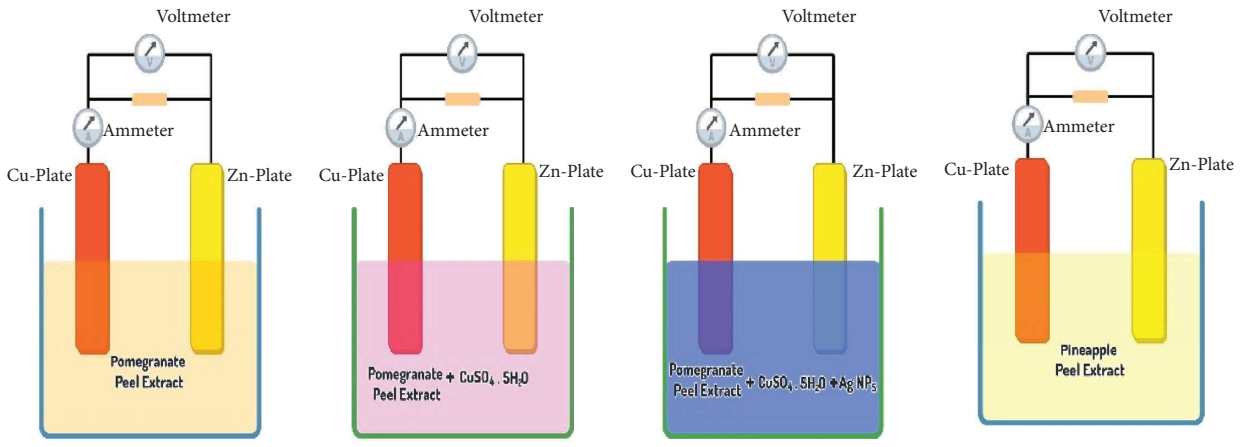

(a) (b) (c) (d)

Figure 3: Continued.

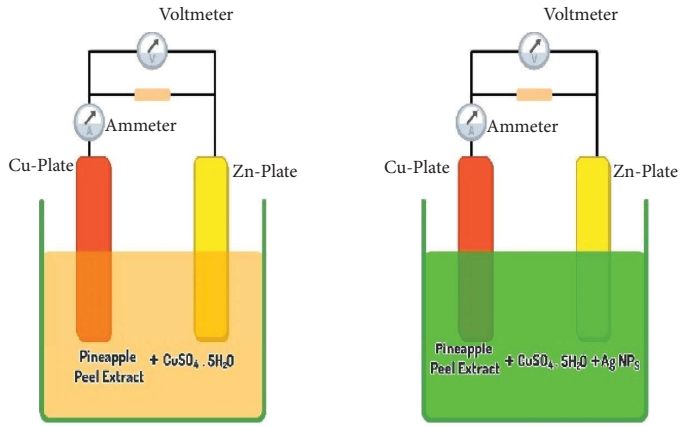

Figure 3: A testing apparatus designed to assess the fundamental concept of PgP and PnP cells utilizing zinc or copper components, (a) electrochemical cell of PgP extract, (b) electrochemical cell of PgP extract with $CuSO_4.5H_2O$ solution, (c) electrochemical cell of PgP and extract with $CuSO_4.5H_2O$ solution and AgNPs, (d) electrochemical cell of PnP extract, (e) electrochemical cell of PnP extract with $CuSO_4.5H_2O$ solution, and (f) electrochemical cell of PnP and extract with $CuSO_4.5H_2O$ solution and AgNPs.

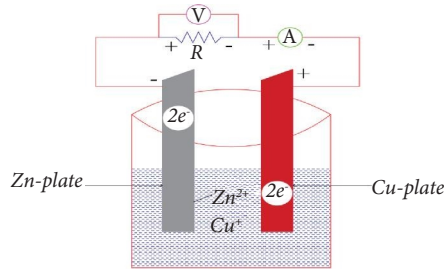

Figure 4: Bioelectrochemical cell chemical reaction.

Total reaction,

$$Zn + Cu^{2+} + 2H^{+} = Zn^{2+} + Cu + H_2, \quad (3)$$

Where Cu^{2+} = reactant ion, H^{+} = ion that reacts, and Zn^{2+} = ion that reacts ion, which undergoes a reaction.

2.8. Analysis of Silver Nanoparticles (AgNPs) Produced through Biological Synthesis. The confirmation of AgNPs formation involved assessing absorbance through a UV-Vis spectrophotometer (UV-VIS-NIR-Shimadzu 2600) within the 200–600 nm wavelength range. In addition, X-ray diffraction (XRD) spectrum analysis was conducted by using an XRD powder method (XRD-ARL EQUINOX 1000, Thermo Scientific) following the established experimental protocol. The transmission electron microscope (TEM) imaging (JOEL JEM-1400) was employed to scrutinize the surface morphology, shape, and elemental composition of AgNPs. Raman spectra were obtained with a Bruker Raman spectrometer (model Raman-Horiba MacroRam, laser source-785 nm). Dynamic light scattering (Malvern Zetasizer Nano-ZS) was used to analyze the particle size of the synthesized AgNPs. For DLS measurements, powder AgNPs were resuspended in distilled water and sonicated for 20–25 minutes to properly disperse the particles in water. With dry and pure KBr crystals, FTIR studies of silver NPs manufactured by PgP and PnP extraction were carried out on the IRPrestige-21 (Kyoto, Japan) of FTIR at 4.0 cm^{-1} determination.

3. Findings and Discourse

3.1. UV-Visible Spectroscopy. The synthesis of silver nanoparticles through the introduction of an alkali solution into the reaction mixture, accompanied by vigorous stirring, demonstrated a rapid generation of these nanoparticles. This process induced a noteworthy color transformation, with the PgP AgNPs transitioning from orange to maroon and the PnP AgNPs changing from light pink to colorless. These alterations served as visible indicators of the successful reduction of $AgNO_3$, marking the formation of the desired nanoparticles [26]. The plasmon resonance of metal nanoparticles, including silver, is highly dependent on their size and shape. Smaller particles may exhibit blue shifts in their localized surface plasmon resonance (LSPR) peaks, potentially falling outside the typical range. The specific synthesis methods and conditions could influence the size and shape of the nanoparticles. Figure 5 shows the UV-Vis absorption spectra showing broad surface plasmon resonance peaks of

(a) PgP extract (navy blue color) and PgP AgNPs (violet color) and (b) PnP extract (pink color) and PnP AgNPs (maroon color). To underscore the environmentally friendly attributes of the AgNPs, their UV absorption spectrum within the 200–600 nm range was meticulously recorded and compared with the UV spectrum of PgP and PnP. The UV-Vis absorption spectra revealed the emergence of distinctive broad surface plasmon resonance peaks at 393 nm and 397 nm for PgP AgNPs and PnP AgNPs, respectively, by established literature data [27–29]. The UV-Vis absorption spectra revealed the emergence of distinctive broad surface plasmon resonance peaks at 291 nm and 297 nm for PgP and PnP extracts, respectively. This observation further corroborated the successful synthesis of silver nanoparticles through the chosen eco-friendly method. Noteworthy variations in absorbance values between the two extracts hinted at subtle differences, possibly attributed to variations in particle size or shape [29]. These nuances are crucial as they provide insights into the characteristics of the synthesized nanoparticles and contribute to the understanding of the synthesis process. The detailed analysis of UV-Vis absorption spectra adds a layer of precision to the assessment of the synthesized AgNPs, reinforcing the credibility of the eco-friendly approach employed in their production.

3.2. XRD Analysis. Upon mixing 9 mL of pomegranate peel (PgP) and pineapple peel (PnP) extracts individually with silver to generate silver nanoparticles (AgNPs), both the extract and the resulting nanoparticles exhibited ten peaks each in their X-ray diffraction (XRD) patterns (refer to Figures 6(a)–6(d)). A typical face-centered cubic structure of PgP has four distinct peaks at 38.36°, 44.62°, 64.98°, and 78.14° for 2 theta values, corresponding to the crystallographic planes (111), (200), (220), and (222) (Figure 6(a)). Similarly, a typical face-centered cubic structure of PnP has four distinct peaks at 36.12°, 42.23°, 60°, and 73° for 2 theta values, corresponding to the crystallographic planes (111), (200), (220), and (222) (Figure 6(c)). A typical face-centered cubic structure of a silver crystal manifests four distinct peaks at 38.38°, 44.45°, 64.81°, and 77.56° for 2 theta values, corresponding to the crystallographic planes (111), (200), (220), and (222) for AgNPs of PgP extract (Figure 6(b)). Similarly, a typical face-centered cubic structure of a silver crystal from pineapple peel extract manifests four distinct peaks at 38.38°, 44.79°, 64.81°, 77.61°, and 81.53° for 2 theta values, corresponding to the crystallographic planes (111), (200), (220), (311), and (220) for AgNPs of PnP extract (Figure 6(d)). These values, consistent with a lattice parameter of $a = 0.386$ nm, align well with the face-centered cubic (FCC) silver reference from the Joint Committee of Powder Diffraction Standard (JCPDS) Card no. 087-0720. The broad, discernible peaks in the XRD patterns suggest a reduction in the size of the AgNPs, indicative of high crystallinity. Additional smaller peaks imply the presence of crystalline organic compounds adsorbed on the surface of the AgNPs, a phenomenon consistent with observations in plant-based synthesis [30]. Applying the Scherrer equation to the XRD pattern [31] enables the calculation of particle size by using the following formula:

$$D = \frac{K\lambda}{\beta \cos\theta}, \tag{4}$$

where D represents the mean size of crystallites (nm), K is the crystallite shape factor (approximately 0.9), λ is the X-ray wavelength, β is the full width at half maximum (FWHM) [32–34] in radians of the X-ray diffraction peak, and θ is the Bragg angle (degrees). By utilizing this equation, the average crystal size of the silver nanoparticles produced by PgP and PnP extracts is reported as 15 nm and 47 nm, respectively. The presence of a significant peak indicates the involvement of bioorganic chemicals and/or proteins throughout the nanoparticle production process. The absence of peaks associated with impurity crystalline phases in the pattern confirms the face-centered cubic form of metallic silver. Noteworthy peaks in the XRD pattern, denoted by "∗," correspond with findings reported in various publications [5, 30, 35–43].

3.3. Raman Spectroscopy. Raman spectroscopy has proven to be a powerful analytical tool in characterizing the structural and vibrational properties of nanoparticles derived from pomegranate peel extract (PgP AgNPs) and pineapple peel extract (PnP AgNPs). The obtained spectra, as illustrated in Figure 7, reveal distinctive peaks that provide valuable insights into the composition and nature of the synthesized nanoparticles. For PgP AgNPs (Figure 7(a)), the Raman spectrum exhibits prominent peaks at 200 cm^{-1}, 231 cm^{-1}, 312 cm^{-1}, 424 cm^{-1}, 468 cm^{-1}, 535 cm^{-1}, 594 cm^{-1}, 650 cm^{-1}, 740 cm^{-1}, 866 cm^{-1}, and 1270 cm^{-1}. These peaks can be attributed to specific vibrational modes associated with the chemical constituents present in the pomegranate peel extract. Such detailed Raman signatures offer a comprehensive understanding of the molecular interactions and bonding configurations within PgP. Similarly, for PnP AgNPs (Figure 7(b)), characteristic peaks are observed at 180 cm^{-1}, 318 cm^{-1}, 422 cm^{-1}, 529 cm^{-1}, 658 cm^{-1}, 735 cm^{-1}, 860 cm^{-1}, 1004 cm^{-1}, and 1270 cm^{-1}.

These peaks correspond to specific vibrational modes associated with the constituents derived from pineapple peel extract, shedding light on the unique chemical composition and structural attributes of PnP AgNPs. In Figure 7(a), the intensive peaks are observed at 1270 cm^{-1}, 866 cm^{-1}, 740 cm^{-1}, and 650 cm^{-1}. These peaks indicate the interaction between the extract and AgNO3 through the carboxylic and hydrophobic groups [44, 45]. The band located at 200 cm^{-1}, 231 cm^{-1}, and 312 cm^{-1} indicates the presence of the silver lattice vibration models [46]. The bands situated at 424 cm^{-1}, 468 cm^{-1}, 535 cm^{-1}, and 594 cm^{-1} indicate the presence of AgNPs for pomegranate peel extract. Similarly, in Figure 7(b), the intensive peaks are observed at 1272 cm^{-1}, 1004 cm^{-1}, and 860 cm^{-1}. These peaks indicate the interaction between the extract and AgNO3 through the carboxylic and hydrophobic groups [44, 45]. The band located at 180 cm^{-1} and 318 cm^{-1} indicates the presence of the silver lattice vibration models [46]. The bands situated at

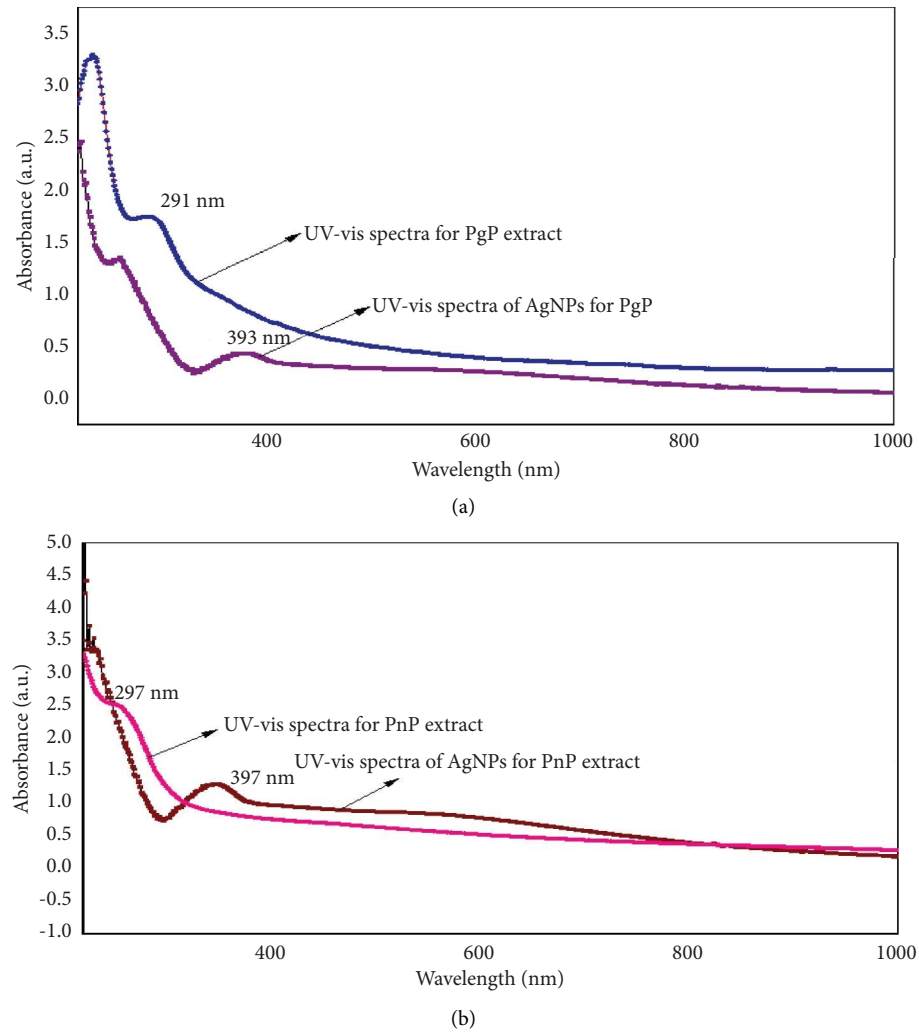

Figure 5: UV-Vis absorption spectra showing broad surface plasmon resonance peaks of (a) PgP and (b) PnP.

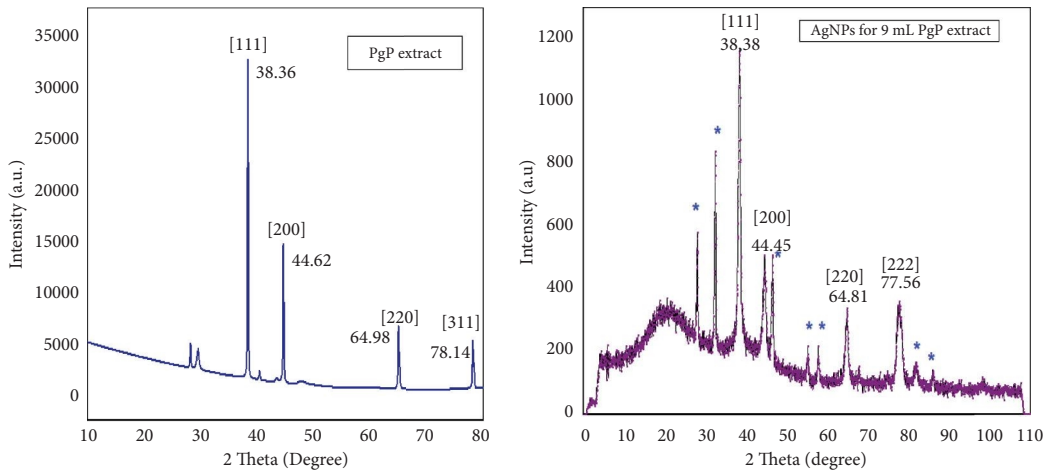

Figure 6: Continued.

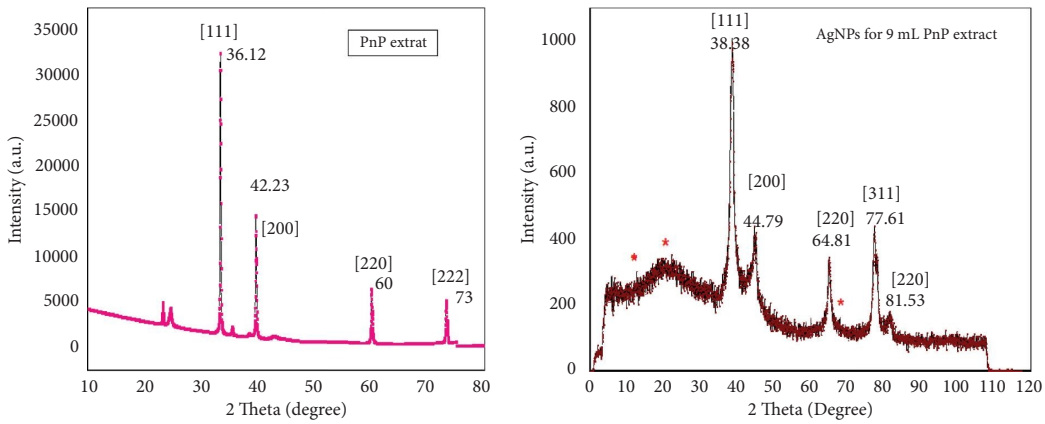

Figure 6: (a) Intensity VS 2 theta for PgP extract, (b) intensity VS 2 theta for synthesized AgNPs for 9 mL PgP, (c) intensity VS 2 theta for PnP extract, and (d) intensity VS 2 theta for synthesized AgNPs for 9 mL PnP.

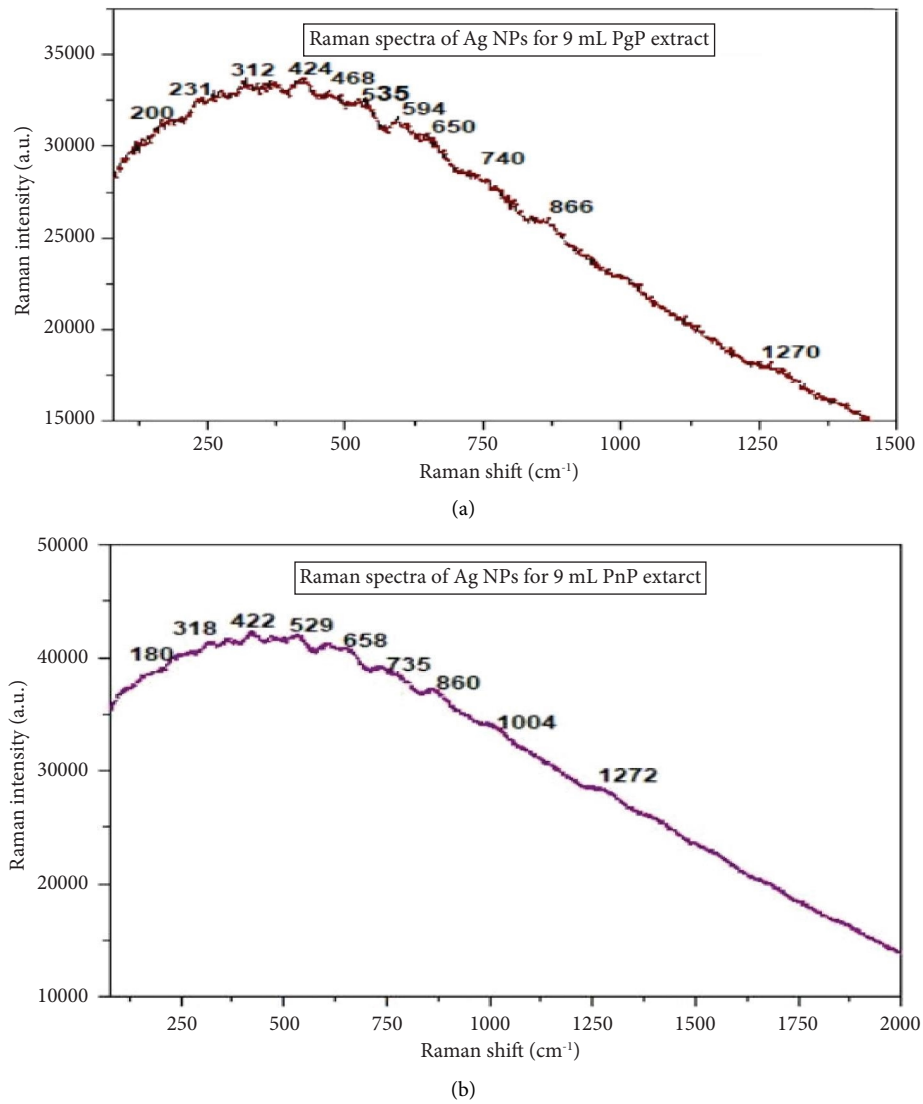

Figure 7: The Raman spectra of the AgNPs of(a) PgP extract-mediated AgNPs for 9 mL and (b) PnP extract-mediated AgNPs for 9 mL.

422 cm^{-1}, 529 cm^{-1}, 658 cm^{-1}, and 735 cm^{-1} indicate the presence of AgNPs for pineapple peel extract. These Raman spectroscopy's findings not only contribute to the characterization of PgP AgNPs and PnP AgNPs but also serve as a foundation for understanding the unique vibrational and structural properties of nanoparticles synthesized from natural extracts. The distinct spectral features provide valuable information for further research and applications in areas such as nanomedicine, catalysis, and sensor technologies.

3.4. TEM Analysis. Figure 8 presents TEM images, particle size distribution histograms, and selected area electron diffraction (SAED) patterns of synthesized AgNPs for 9 mL PnP and synthesized AgNPs for 9 mL PgP. From the TEM images shown in Figures 8(a) and 8(d), there are lots of defect sites that can be observed on the surface of the composite as well as explained nanoparticles. The particle size distribution histogram was constructed based on the analysis of 52 nanoparticles. In Figure 8(b), the mean size of the PnP particles is 37 nm with a standard deviation of 11 nm. Figure 8(e) illustrates that the mean size of the PgP particles is 24 nm with a standard deviation of 9 nm. Furthermore, a noticeable reduction in agglomeration is observed, and smaller-sized particles are fabricated. From XRD analysis, by applying the Debye–Scherrer equation, the average crystalline size of the silver nanoparticles produced by PnP and PgP extracts is reported as 47 nm and 15 nm, respectively, which is in an agreement with the result obtained from the TEM images [47, 48]. The selected area electron diffraction (SAED) pattern supports this, indicating a fully crystalline structure with multiple lattice plane reflections. In the SAED pattern of the AgNPs for 9 mL PnP in Figure 8(c), concentric circles are observed, indexed as (111), (200), (220), and (311) lattice planes, and for the synthesized AgNPs for 9 mL PgP in Figure 8(f), concentric circles are observed, indexed as (111), (200), (220), and (222). These circles correspond well with the XRD data. Therefore, the SAED pattern indicates that synthesized AgNPs for 9 mL PnP and synthesized AgNPs for 9 mL PgP nanoparticles possess a fully crystalline structure. A comparative assessment between TEM images and XRD studies indicates that the extract significantly influences nanoparticle size, playing a crucial role in controlling the size reduction process.

3.5. FTIR Study. The FTIR spectroscopy analysis was studied to hypothesize the possible biomolecules of PgP and PnP extracts responsible for the synthesis of AgNPs. In Figure 9(a), there is a deviation of peak observed for PgP AgNPs at 3334 cm^{-1} and 1626 cm^{-1}. It suggests that the O-H and C=O groups were adsorbed on the surface of AgNPs and involved in the reduction process. In Figure 9(c), there is a deviation of peak observed for PnP AgNPs at 3342 cm^{-1} and 1650 cm^{-1}. It suggests that the O-H and C=O groups were adsorbed on the surface of AgNPs and involved in the reduction process. The peaks near 3324 cm^{-1}, 2126 cm^{-1}, and 1634 cm^{-1} (Figure 9(b)) could be due to the O-H, aliphatic C=H, and C=O stretching vibrations of flavonoids/phenolic groups. The peak at 1224 cm^{-1} corresponds to the O-H bend of polyphenol and confirms the presence of an aromatic group, whereas the absorption peaks at 1132 cm^{-1} were assigned for C-O-C and secondary -OH groups [49] of PgP AgNPs. The peaks near 3344 cm^{-1}, 2142 cm^{-1}, and 1634 cm^{-1} (Figure 9(d)) could be due to the O-H, aliphatic C=H, and C=O stretching vibrations of flavonoids/phenolic groups. The peak at 1222 cm^{-1} corresponds to the O-H bend of polyphenol and confirms the presence of an aromatic group, whereas the absorption peaks at 1096 cm^{-1} were assigned for C-O-C and secondary -OH groups [49] of PnP AgNPs. Table 1 depicts the FTIR analysis with wavenumber and functional group.

3.6. DLS Analysis. Figure 10 shows the size distribution profile of these biosynthesized silver nanoparticles of PgP and PnP AgNPs for 9 mL. The AgNPs were found to have a size distribution ranging from 1 to 100 nm. The DLS study is required to investigate the particle size in colloidal solution and the curve obtained by scanning the suspension of Ag nanoparticles indicates the average size (diameter) of the silver nanoparticles to be around 21 nm for PgP AgNPs and 50 nm for PnP AgNPs, which confirmed the good stability of AgNPs [49, 50].

3.7. Functioning of the Summary Units for the Production of Electrical Power. Silver nanoparticles (AgNPs) synthesized through green methods were employed in a bioelectrochemical cell to assess their impact on a power generation system. Figure 11 illustrates the influence of AgNPs on three distinct scenarios in the bioelectrochemical cell, utilizing PgP and PnP extracts. In Figure 11(a), changes in open circuit voltage over time are depicted across various scenarios. Scenario 3 consistently shows higher open circuit voltages than scenarios 2 and 3. Specifically, in scenario 1 (PgP extract), the voltage fluctuates over 700 hours, ranging from a maximum of 4.18 V to a minimum of 4.05 V. Scenario 2 (PgP extract + $CuSO_4.5H_2O$) achieves a maximum open circuit voltage of 5.49 V and a minimum of 5 V, while scenario 3 (PgP + $CuSO_4.5H_2O$ + NPs) reaches a maximum of 6.89 V and a minimum of 6 V. These results imply that the presence of nanoparticles may enhance the open circuit voltage. In Figure 11(b), the short-circuit current over time is presented for different scenarios, revealing that scenario 3 consistently generates a higher short-circuit current than scenarios 2 and 3. In scenario 1 (PgP extract), the short-circuit current varies over 700 hours, with a maximum of 1.94 mA and a minimum of 1.85 mA. Scenario 2 (PgP extract + $CuSO_4.5H_2O$) achieves a maximum short-circuit current of 2.99 mA and a minimum of 2.86 mA, while scenario 3 (PgP extract + $CuSO_4.5H_2O$ + NPs) reaches a maximum of 3.99 mA and a minimum of 3.82 mA. This indicates that AgNPs may play a significant role in increasing the short-circuit current of the pomegranate bioelectrochemical cell over time. Figure 11(c) presents the estimated power output of the cells over time. Scenario 3 yields the highest maximum power of 15.99 W and a minimum of 15.71 W, while scenario 2 and scenario 1 reach

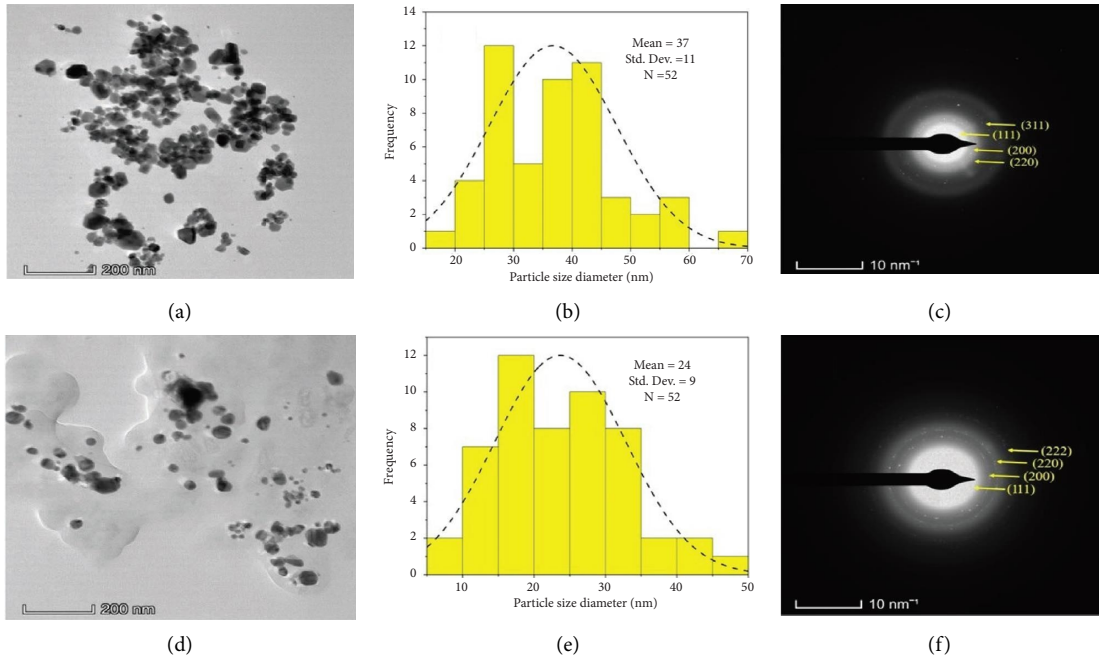

Figure 8: TEM images of (a) AgNPs for 9 mL PnP and (d) AgNPs for 9 mL PgP, particle size distribution histogram of (b) AgNPs for 9 mL PnP and (e) AgNPs for 9 mL PgP, and SAED pattern of (c) AgNPs for 9 mL PnP and (f) AgNPs for 9 mL PgP.

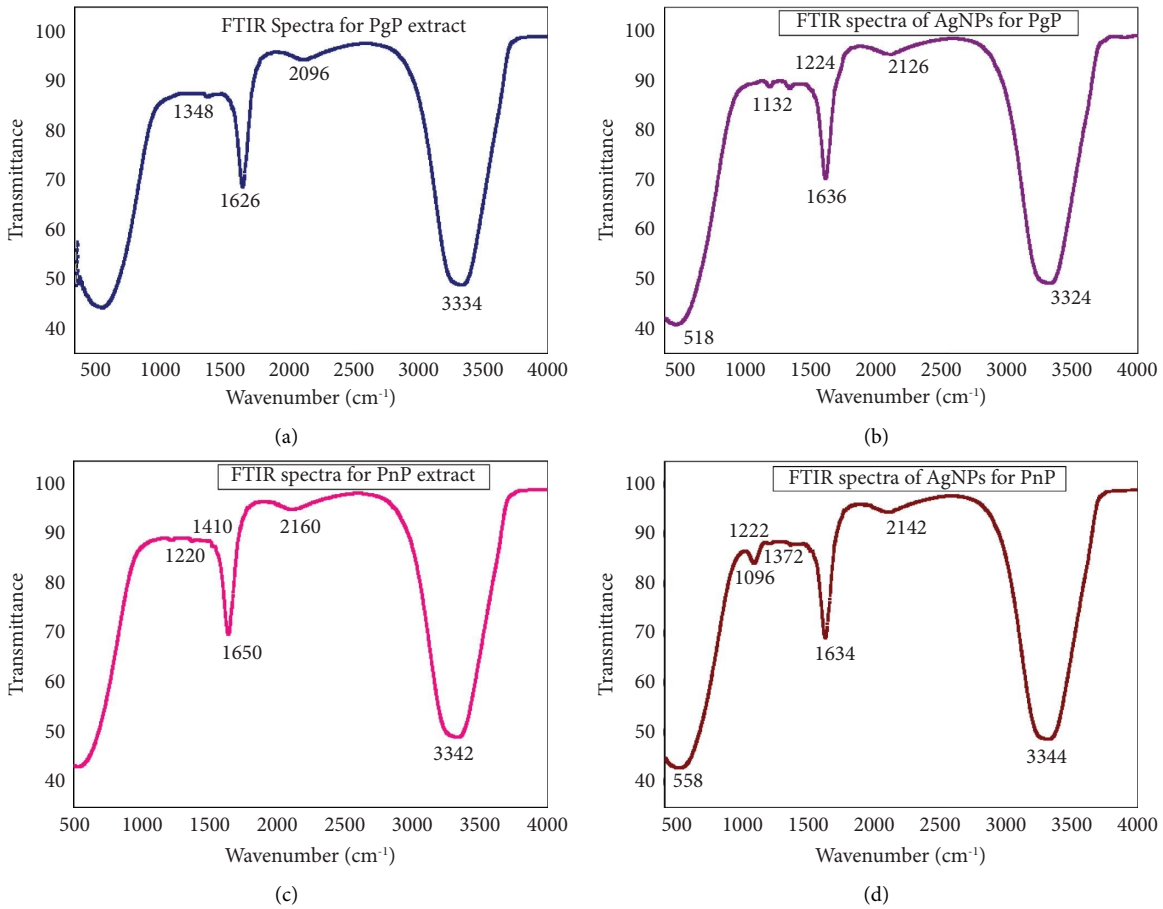

Figure 9: FTIR spectra of (a) PgP extract, (b) AgNPs for PgP, (c) PnP extract, and (d) AgNPs for PnP.

Table 1: FTIR analysis with wavenumber and functional group.

Wavenumber (cm^{-1})				Functional group
PgP extract	PgP AgNPs	PnP extract	PnP AgNPs	
3334	3324	3342	3344	O-H stretching
1626	1634	1650	1634	C=O stretching
	2126		2142	C=H stretching
	1224		1222	O-H bending
	1132		1096	C-O-C and secondary -OH group

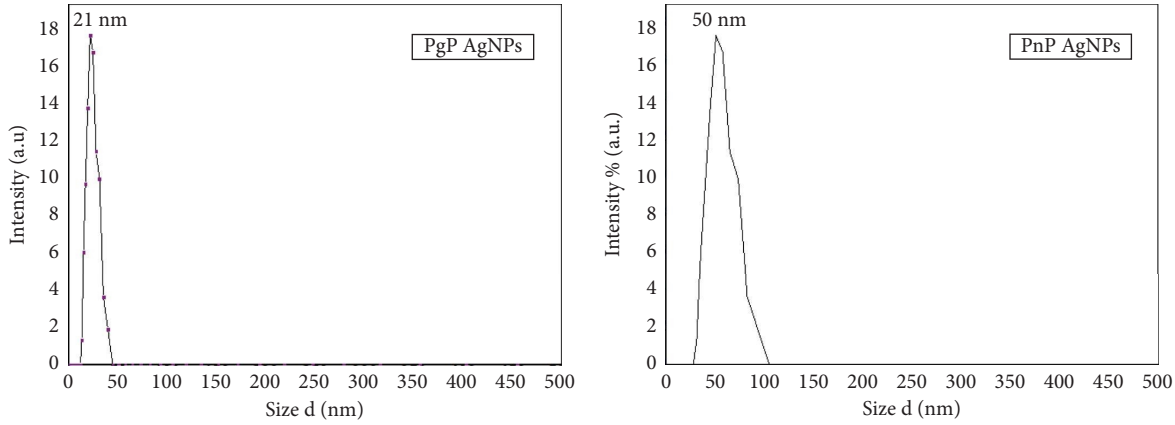

(a) (b)

Figure 10: The size distribution profile of these biosynthesized silver nanoparticles of (a) PgP extract-mediated AgNPs for 9 mL and (b) PnP extract-mediated AgNPs for 9 mL.

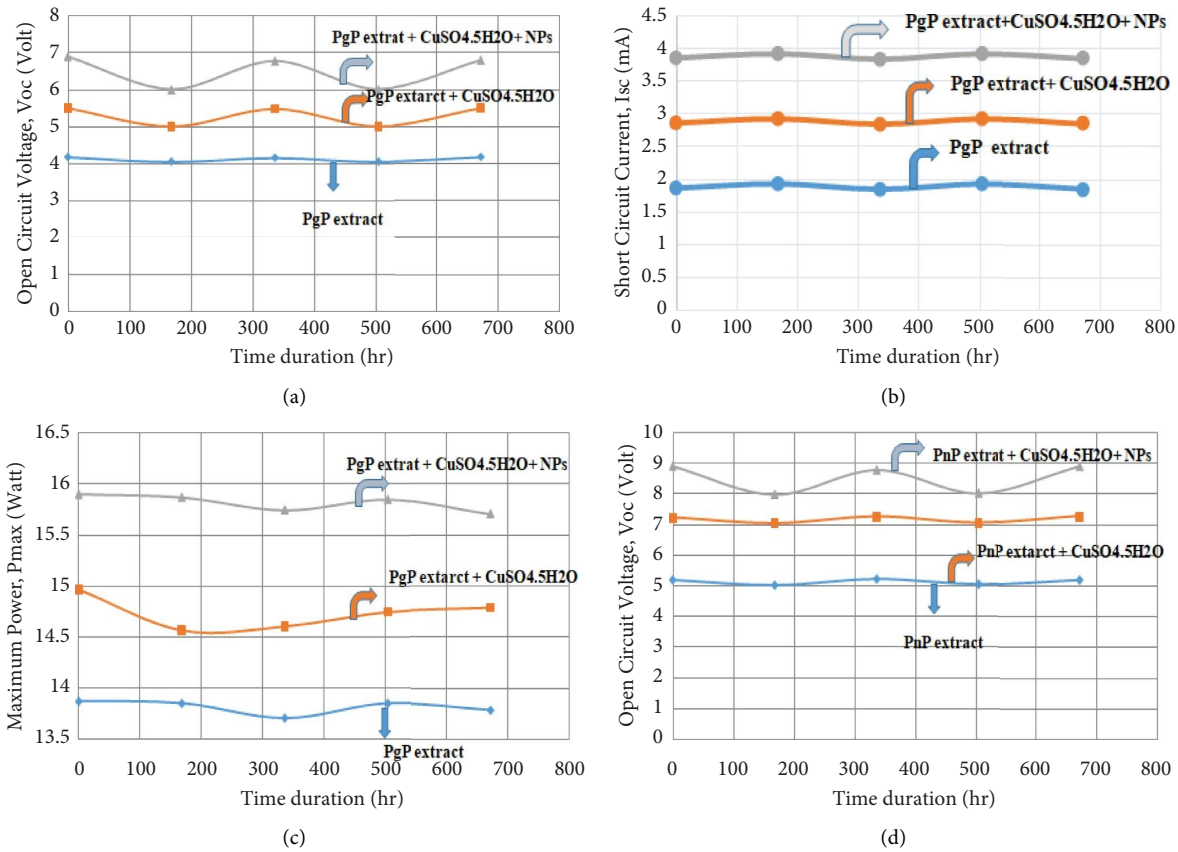

(a) (b)

(c) (d)

Figure 11: Continued.

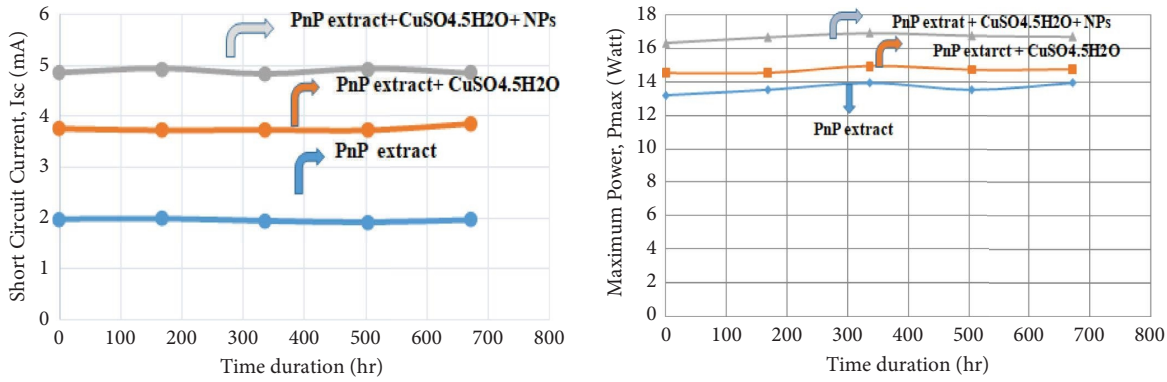

FIGURE 11: The influence of AgNPs on three distinct scenarios in the bioelectrochemical cell, utilizing PgP and PnP extracts: (a) open-circuit voltage for PgP, (b) short-circuit current for PgP, (c) maximum power for PgP, (d) open-circuit voltage for PnP, (e) short-circuit current for PnP, and (f) maximum power for PnP.

a maximum power of 14.70 W and 14.99 W, respectively, with minimum power values of 13.72 W and 13.87 W, respectively. The addition of AgNPs to the PgP extract's bioelectrochemical cell results in the highest power output, remaining stable for 700 hours. In Figure 11(d), changes in open circuit voltage over time are depicted across various scenarios. Scenario 3 consistently shows higher open circuit voltages than scenarios 2 and 1. Specifically, in scenario 1 (PnP extract), the voltage fluctuates over 700 hours, ranging from a maximum of 5.21 V to a minimum of 5.02 V. Scenario 2 (PgP extract + $CuSO_4.5H_2O$) achieves a maximum open circuit voltage of 7.26 V and a minimum of 7.03 V, while scenario 3 (PnP + $CuSO_4.5H_2O$ + NPs) reaches a maximum of 8.89 V and a minimum of 7.98 V. These results imply that the presence of nanoparticles may enhance the open circuit voltage. In Figure 11(e), the short-circuit current over time is presented for different scenarios, revealing that scenario 3 consistently generates a higher short-circuit current than scenarios 2 and 3. In scenario 1 (PnP extract), the short-circuit current varies over 700 hours, with a maximum of 1.98 mA and a minimum of 1.92 mA. Scenario 2 (PnP extract + $CuSO_4.5H_2O$) achieves a maximum short-circuit current of 3.86 mA and a minimum of 3.74 mA, while scenario 3 (PnP extract + $CuSO_4.5H_2O$ + NPs) reaches a maximum of 4.94 mA and a minimum of 4.86 mA. This indicates that AgNPs may play a significant role in increasing the short-circuit current of the pomegranate bioelectrochemical cell over time. Figure 11(f) presents the estimated power output of the cells over time. Scenario 3 yields the highest maximum power of 16.93 W and a minimum of 16.32 W, while scenario 2 and scenario 1 reach a maximum power of 14.97 W and 13.99 W, respectively, with minimum power values of 14.56 W and 13.21 W. The addition of AgNPs to the PnP extract's bioelectrochemical cell results in the highest power output, remaining stable for 700 hours. These findings underscore the potential of AgNPs to enhance power generation in bioelectrochemical cells of PgP and PnP separately. The open circuit voltage and short-circuit current improve swiftly following the addition of AgNPs, resulting in a significant enhancement in power output for the pomegranate bioelectrochemical cells of PgP and PnP separately. These findings suggest that the use of AgNPs in bioelectrochemical cells holds great promise for future applications in power generation.

The study underscores the potential of AgNPs to enhance power generation in bioelectrochemical cells using PgP and PnP extracts. The swift improvements in open circuit voltage and short-circuit current following the addition of AgNPs suggest a significant enhancement in power output for both types of pomegranate's bioelectrochemical cells. These findings imply that the use of AgNPs holds promise for future applications in power generation, showcasing the feasibility of incorporating green-synthesized nanoparticles into bioelectrochemical systems.

4. Conclusion

Silver nanoparticles (AgNPs) were successfully synthesized for the first time using a rapid, cost-effective, and environmentally friendly approach involving pomegranate peel and pineapple peel extracts with a comparative study. The reduction of Ag^+ to Ag0 was confirmed by the highest ultraviolet-visible absorbance at 360 nm for pomegranate peel and 390 nm for pineapple peel in the silver nanoparticles. The Raman spectra of AgNPs revealed active functionalization groups crucial for their reduction. Employing biological processes led to the formation of spherical Ag nanoparticles with an average size of 15 nm for pomegranate peel and 47 nm for pineapple peel. The TEM analysis discovered that the biologically synthesized silver nanoparticles were well dispersed with no agglomeration. The size of nanoparticles ranges from 10 to 200 nm with different shapes such as spherical, triangular, hexagonal, and rod. Active functionalization groups that are crucial to the reduction of silver nanoparticles were discovered in the Raman spectra of AgNPs. While previous research has explored eco-friendly methods for producing silver nanoparticles using various plant components, this study introduced a novel aspect by investigating the impact of AgNPs on the lifespan of energy-generating organisms.

Notably, electrochemical cells were introduced in this experiment. The resulting AgNPs were found to enhance the longevity of pomegranate peel and pineapple peel extracts electrochemical cells in terms of energy generation. This discovery holds promise for characterizing and understanding the durability of electrochemical cell-mediated nanoparticle production for plant-based applications, especially in the context of prolonged use in high-quality power generators. The findings suggest a need for further exploration into how organic cells contribute to energy generation.

Data Availability

Data sharing does not apply to this article as no datasets were generated or analyzed during the current study

Conflicts of Interest

The authors declare that they have no conflicts of interest.

Authors' Contributions

Shamima Mehrin conceptualized and investigated the study, proposed the methodology, collected the resources, wrote the original draft, and reviewed and edited the manuscript. N. Y. Tanisa and Rabiul Awal curated the data, performed the formal analysis, proposed the methodology, and reviewed and edited the manuscript. Kamrul Alam Khan, Shamim Ahmed, Shahidul Islam, Asad Mia, and Abdus Shaqur reviewed and edited the manuscript.

References

[1] I. Hussain, M. Brust, A. J. Papworth, and A. I. Cooper, "Preparation of acrylate-stabilized gold and silver hydrosols and gold-polymer composite films," *Langmuir*, vol. 19, no. 11, pp. 4831–4835, 2003.

[2] M. D. Cheng, "Effects of nanophase materials (≤20 nm) on biological responses," *Journal of Environmental Science and Health, Part A*, vol. 39, no. 10, pp. 2691–2705, 2004.

[3] T. Masciangioli and W. X. Zhang, *Peer Reviewed: Environmental Technologies At The Nanoscale*, ACS Publications, Washington, DC, USA, 2003.

[4] M. A. Albrecht, C. W. Evans, and C. L. Raston, "Green chemistry and the health implications of nanoparticles," *Green Chemistry*, vol. 8, no. 5, pp. 417–432, 2006.

[5] N. Y. Tanisa, M. K. Alam khan, and M. Salahuddin, "Green production and analysis of silver nanoparticles utilizing Pathor Kuchi Leaf," *AIP Advances*, vol. 13, no. 9, 2023.

[6] A. M. P. Rivera, C. R. Toro, L. Londoño, G. Bolivar, J. A. Ascacio, and C. N. Aguilar, "Bioprocessing of pineapple waste biomass for sustainable production of bioactive compounds with high antioxidant activity," *Journal of Food Measurement and Characterization*, vol. 17, no. 1, pp. 586–606, 2023.

[7] G. Vasyliev, V. Vorobyova, M. Skiba, and L. Khrokalo, "Green synthesis of silver nanoparticles using waste products (apricot and black currant pomace) aqueous extracts and their characterization," *Advances in Materials Science and Engineering*, vol. 2020, Article ID 4505787, 11 pages, 2020.

[8] G. Lakshmanan, A. Sathiyaseelan, K. Pt, and K. Murugesan, "Plant-mediated synthesis of silver nanoparticles using fruit extract of Cleome viscosa L.: assessment of their antibacterial and anticancer activity," *Karbala International Journal of Modern Science*, vol. 4, no. 1, pp. 61–68, 2018.

[9] H. F. Aritonang, H. Koleangan, and A. D. Wuntu, "Synthesis of silver nanoparticles using aqueous extract of medicinal plants'(Impatiens balsamina and Lantana camara) fresh leaves and analysis of antimicrobial activity," *International journal of microbiology*, vol. 2019, Article ID 8642303, 8 pages, 2019.

[10] M. Iftikhar, M. Zahoor, S. Naz et al., "Green synthesis of silver nanoparticles using Grewia optiva leaf aqueous extract and isolated compounds as reducing agent and their biological activities," *Journal of Nanomaterials*, vol. 2020, Article ID 8949674, 10 pages, 2020.

[11] A. Ejaz, Z. Mamtaz, I. Yasmin et al., "Cyperus scariosus extract based greenly synthesized gold nanoparticles as colorimetric nanoprobe for Ni2+ detection and as antibacterial and photocatalytic agent," *Journal of Molecular Liquids*, vol. 393, Article ID 123622, 2024.

[12] S. Pirtarighat, M. Ghannadnia, and S. Baghshahi, "Green synthesis of silver nanoparticles using the plant extract of Salvia spinosa grown in vitro and their antibacterial activity assessment," *Journal of Nanostructure in Chemistry*, vol. 9, pp. 1–9, 2019.

[13] A. Jabbar, A. Abbas, N. Assad et al., "A highly selective Hg 2+ colorimetric sensor and antimicrobial agent based on green synthesized silver nanoparticles using Equisetum diffusum extract," *RSC Advances*, vol. 13, no. 41, pp. 28666–28675, 2023.

[14] A. B. Siddique, D. Amr, A. Abbas et al., "Synthesis of hydroxyethylcellulose phthalate-modified silver nanoparticles and their multifunctional applications as an efficient antibacterial, photocatalytic and mercury-selective sensing agent," *International Journal of Biological Macromolecules*, vol. 256, Article ID 128009, 2024.

[15] M. I. Irfan, F. Amjad, A. Abbas et al., "Novel carboxylic acid-capped silver nanoparticles as antimicrobial and colorimetric sensing agents," *Molecules*, vol. 27, no. 11, p. 3363, 2022.

[16] M. S. Mohseni, M. A. Khalilzadeh, M. Mohseni et al., "Green synthesis of Ag nanoparticles from pomegranate seeds extract and synthesis of Ag-Starch nanocomposite and characterization of mechanical properties of the films," *Biocatalysis and Agricultural Biotechnology*, vol. 25, Article ID 101569, 2020.

[17] M. Govindappa, S. Tejashree, V. Thanuja et al., "Pomegranate fruit fleshy pericarp mediated silver nanoparticles possessing antimicrobial, antibiofilm formation, antioxidant, biocompatibility and anticancer activity," *Journal of Drug Delivery Science and Technology*, vol. 61, Article ID 102289, 2021.

[18] A. Baran, C. Keskin, M. F. Baran et al., "Ecofriendly synthesis of silver nanoparticles using ananas comosus fruit peels: anticancer and antimicrobial activities," *Bioinorganic Chemistry and Applications*, vol. 2021, Article ID 2058149, 8 pages, 2021.

[19] N. Assad, M. Naeem-ul-Hassan, M. Ajaz Hussain et al., "Diffused sunlight assisted green synthesis of silver nanoparticles using Cotoneaster nummularia polar extract for antimicrobial and wound healing applications," *Natural Product Research*, pp. 1–15, 2023.

[20] S. Ullah, R. Khalid, M. F. Rehman et al., "Biosynthesis of phyto-functionalized silver nanoparticles using olive fruit extract and evaluation of their antibacterial and antioxidant

properties," *Frontiers in Chemistry*, vol. 11, Article ID 1202252, 2023.

[21] A. Ravindran, P. Chandran, and S. S. Khan, "Biofunctionalized silver nanoparticles: advances and prospects," *Colloids and Surfaces B: Biointerfaces*, vol. 105, pp. 342–352, 2013.

[22] M. K. Choudhary, J. Kataria, S. S. Cameotra, and J. Singh, "A facile biomimetic preparation of highly stabilized silver nanoparticles derived from seed extract of Vigna radiata and evaluation of their antibacterial activity," *Applied Nanoscience*, vol. 6, no. 1, pp. 105–111, 2016.

[23] X. F. Zhang, Z. G. Liu, W. Shen, and S. Gurunathan, "Silver nanoparticles: synthesis, characterization, properties, applications, and therapeutic approaches," *International Journal of Molecular Sciences*, vol. 17, no. 9, p. 1534, 2016.

[24] B. Wiley, Y. Sun, and Y. Xia, "Synthesis of silver nanostructures with controlled shapes and properties," *Accounts of Chemical Research*, vol. 40, no. 10, pp. 1067–1076, 2007.

[25] S. Amin, M. Sher, A. Ali et al., "Sulfonamide-functionalized silver nanoparticles as an analytical nanoprobe for selective Ni (II) sensing with synergistic antimicrobial activity," *Environmental Nanotechnology, Monitoring & Management*, vol. 18, Article ID 100735, 2022.

[26] P. Logeswari, S. Silambarasan, and J. Abraham, "Ecofriendly synthesis of silver nanoparticles from commercially available plant powders and their antibacterial properties," *Scientia Iranica*, vol. 20, no. 3, pp. 1049–1054, 2013.

[27] S. Iravani, H. Korbekandi, S. V. Mirmohammadi, and B. Zolfaghari, "Synthesis of silver nanoparticles: chemical, physical and biological methods," *Research in pharmaceutical sciences*, vol. 9, no. 6, pp. 385–406, 2014.

[28] A. Oraibi, R. Mohsien, W. Atea, H. Yahia, and L. Raheem, "Antibacterial activity of silver nanoparticles and Pomegranate (Punica granatum L.) extracts," *International Journal of Current Microbiology and Applied Sciences*, vol. 5, no. 12, pp. 131–140, 2016.

[29] P. Banerjee, M. Satapathy, A. Mukhopahayay, and P. Das, "Leaf extract mediated green synthesis of silver nanoparticles from widely available Indian plants: synthesis, characterization, antimicrobial property and toxicity analysis," *Bioresources and Bioprocessing*, vol. 1, pp. 3–10, 2014.

[30] S. M. Hasan, N. Y. Tanisa, S. Ahmed, M. ArifurRahman, and R. Awal, "Producing and assessing zinc sulfate nanoparticles using Nigella sativa assistance," *AIP Advances*, vol. 13, no. 12, 2023.

[31] S. J. Joshi, S. J. Geetha, S. Al-Mamari, and A. Al-Azkawi, "Green synthesis of silver nanoparticles using pomegranate peel extracts and its application in photocatalytic degradation of methylene blue," *Jundishapur Journal of Natural Pharmaceutical Products*, vol. 13, no. 3, 2018.

[32] N. Jayaprakash, J. J. Vijaya, K. Kaviyarasu et al., "Green synthesis of Ag nanoparticles using Tamarind fruit extract for the antibacterial studies," *Journal of Photochemistry and Photobiology B: Biology*, vol. 169, pp. 178–185, 2017.

[33] A. Leela and M. Vivekanandan, "Tapping the unexploited plant resources for the synthesis of silver nanoparticles," *African Journal of Biotechnology*, vol. 7, no. 17, 2008.

[34] S. S. Shankar, A. Rai, A. Ahmad, and M. Sastry, "Rapid synthesis of Au, Ag, and bimetallic Au core–Ag shell nanoparticles using Neem (Azadirachta indica) leaf broth," *Journal of Colloid and Interface Science*, vol. 275, no. 2, pp. 496–502, 2004.

[35] J. L. Gardea-Torresdey, J. G. Parsons, E. Gomez et al., "Formation and growth of Au nanoparticles inside live alfalfa plants," *Nano Letters*, vol. 2, no. 4, pp. 397–401, 2002.

[36] R. Parameshwaran, S. Kalaiselvam, and R. Jayavel, "Green synthesis of silver nanoparticles using Beta vulgaris: role of process conditions on size distribution and surface structure," *Materials Chemistry and Physics*, vol. 140, no. 1, pp. 135–147, 2013.

[37] P. Das, K. Ghosal, N. K. Jana, A. Mukherjee, and P. Basak, "Green synthesis and characterization of silver nanoparticles using belladonna mother tincture and its efficacy as a potential antibacterial and anti-inflammatory agent," *Materials Chemistry and Physics*, vol. 228, pp. 310–317, 2019.

[38] D. Kalpana and Y. S. Lee, "Synthesis and characterization of bactericidal silver nanoparticles using cultural filtrate of simulated microgravity grown Klebsiella pneumoniae," *Enzyme and Microbial Technology*, vol. 52, no. 3, pp. 151–156, 2013.

[39] N. Aziz, M. Faraz, R. Pandey et al., "Facile algae-derived route to biogenic silver nanoparticles: synthesis, antibacterial, and photocatalytic properties," *Langmuir*, vol. 31, no. 42, pp. 11605–11612, 2015.

[40] V. S. Suvith and D. Philip, "Catalytic degradation of methylene blue using biosynthesized gold and silver nanoparticles," *Spectrochimica Acta Part A: Molecular and Biomolecular Spectroscopy*, vol. 118, pp. 526–532, 2014.

[41] S. Hamedi, S. A. Shojaosadati, and A. Mohammadi, "Evaluation of the catalytic, antibacterial and anti-biofilm activities of the Convolvulus arvensis extract functionalized silver nanoparticles," *Journal of Photochemistry and Photobiology B: Biology*, vol. 167, pp. 36–44, 2017.

[42] K. Anandalakshmi, J. Venugobal, and V. J. A. N. Ramasamy, "Characterization of silver nanoparticles by green synthesis method using Pedalium murex leaf extract and their antibacterial activity," *Applied Nanoscience*, vol. 6, no. 3, pp. 399–408, 2016.

[43] C. Wu, X. Zhou, and J. Wei, "Localized surface plasmon resonance of silver nanotriangles synthesized by a versatile solution reaction," *Nanoscale Research Letters*, vol. 10, pp. 354–356, 2015.

[44] Z. Salari, F. Danafar, S. Dabaghi, and S. A. Ataei, "Sustainable synthesis of silver nanoparticles using macroalgae Spirogyra varians and analysis of their antibacterial activity," *Journal of Saudi Chemical Society*, vol. 20, no. 4, pp. 459–464, 2016.

[45] M. Ali, B. Kim, K. D Belfield, D. Norman, M. Brennan, and G. S. Ali, "Green synthesis and characterization of silver nanoparticles using Artemisia absinthium aqueous extract—a comprehensive study," *Materials Science and Engineering: C*, vol. 58, pp. 359–365, 2016.

[46] M. Nasiriboroumand, M. Montazer, and H. Barani, "Preparation and characterization of biocompatible silver nanoparticles using pomegranate peel extract," *Journal of Photochemistry and Photobiology B: Biology*, vol. 179, pp. 98–104, 2018.

[47] Z. Izadiyan, K. Shameli, M. Miyake et al., "Cytotoxicity assay of plant-mediated synthesized iron oxide nanoparticles using Juglans regia green husk extract," *Arabian Journal of Chemistry*, vol. 13, no. 1, pp. 2011–2023, 2020.

[48] B. Kumar, K. Smita, L. Cumbal, A. Debut, and Y. Angulo, "Biofabrication of copper oxide nanoparticles using Andean blackberry (Rubus glaucus Benth.) fruit and leaf," *Journal of Saudi Chemical Society*, vol. 21, pp. S475–S480, 2017.

[49] S. V. Patil, H. P. Borase, C. D. Patil, and B. K. Salunke, "Biosynthesis of silver nanoparticles using latex from few euphorbian plants and their antimicrobial potential," *Applied Biochemistry and Biotechnology*, vol. 167, no. 4, pp. 776–790, 2012.

[50] N. Y. Tanisa, K. A. Khan, and M. Salahuddin, "Synthesis, evaluation, and monitoring of red amaranth extract for power production," *Advances in Natural Sciences: Nanoscience and Nanotechnology*, vol. 15, no. 1, Article ID 015001, 2024.